



# RC Beams under Blast Loads: Numerical Simulation and Machine Learning Modeling

Received 17 December 2023; Revised 19 February 2024; Accepted 1 March 2024

Mahmoud A. Samak<sup>1</sup>,  
Ehab M. Lotfy<sup>2</sup>,  
Erfan E. Abdel Latif<sup>3</sup>,  
Manar A. Ahmed<sup>4\*</sup>

## Keywords

Explosion waves;  
Strain rate; Failure  
mode; ABAQUS  
simulation of RC  
beams; ANN modeling.

**Abstract:** The use of explosives to target civilian buildings and other structures around the world is becoming a growing problem in modern societies. This paper focuses on RC beams exposed to free-air blast loads. The paper first presents a parametric study on the behavior of RC beams subjected to blast loads using finite element simulation and then proposes an Artificial Neural Network (ANN) model to predict that behavior in a simple and easy manner. The ABAQUS program is used to simulate RC beams under blast loads. Experimental data was collected from the literature and used to validate the ABAQUS models. Deflection, reaction forces, ultimate stress, ultimate strain, and failure mode of RC beams are investigated. The considered design parameters in the parametric study are the characteristic compressive strength of concrete ( $f_{cu}$ ), the transverse reinforcement ratio ( $\rho_T\%$ ), the longitudinal reinforcement ratio ( $\rho_L\%$ ), and the scaled distance ( $Z$ ). In this paper, the proposed ANN model was trained and tested using datasets produced using ABAQUS. The input parameters of the ANN model are TNT weight, standoff distance ( $D$ ), characteristic compressive strength of concrete, transverse reinforcement ratio, longitudinal reinforcement ratio, width-to-thickness ratio ( $b/t$ ), and length-to-thickness ratio ( $L/t$ ). The predicted behavior using the ANN model showed the credibility of the model. The results indicated that  $L/t$ ,  $b/t$ , and  $Z$  have significant effects on the behavior of RC beams under blast loads compared with  $f_{cu}$ ,  $\rho_T\%$ , and  $\rho_L\%$ , the cracks area increases with the decrease in  $Z$ ,  $f_{cu}$ , and  $b/t$  and decreases with  $L/t$  decrease.

## 1. Introduction

Several building structures may be exposed to blast loads because of natural or human-caused events. The importance of protecting the existing structures from the impact of

<sup>1</sup> Civil Engineering Department, Faculty of Engineering, Suez Canal University

<sup>2</sup> Civil Engineering Department, Faculty of Engineering, Suez Canal University

<sup>3</sup> Civil Engineering Department, Faculty of Engineering, Suez Canal University

<sup>4</sup> Civil Engineering Department, Faculty of Engineering, Suez Canal University, Ismailia, Ismailia

explosions presents a particular challenge. This field has become one of the most important areas when designing buildings to withstand explosive loads in various countries [1-3]. Many experimental studies have been performed on the blast response of RC members. Zhao et al. [4] investigated the damaged area of an RC beam under a rectangular contact explosion through tests of full-scale beam and numerical simulation. A calculation equation of beam damage area was proposed. The result of the contact explosion damaged area under a mass of 1 to 6 kg of TNT showed that the damage in the width direction is greater than that in the span direction. Gomes et al. [5] carried out full-scaled blast testing experimental tests to investigate the effect of blast energy-absorbing connectors (EACs) on building structures. LS-DYNA finite element numerical model was used to analyze the response of a simple idealized reinforced concrete structure under three blast-loading scenarios (far-field, near-field, and very near-field explosions) to assess the effect of standoff distance on the effectiveness of the protective system. EACs strongly limit the forces imparted to the protected structure and significantly reduce the corresponding energy absorption demand, especially for near-field explosions. Robert et al. [6] conducted a full-scale blast test to investigate the capacity of light steel-based wall panels to resist the effects of external explosions. Etabs numerical model has been also calibrated. The results showed that the ultimate capacity of the wall panels is strongly dependent on the initial design conditions and panel-to-structure fastening solution. Chaozhi et al. [7] presented an analytical model to investigate the dimensions of the damage zone on the blasting surface of RC beams under contact explosion. By comparing the analytical model with experimental results, an average error of 9.05 % is observed for the analytical model.

Chuanjing et al. [8] presented an experimental study on the effect of strengthening configuration on the blast behavior of UHPFRC retrofitted RC beams tested under single and repeated blast loads using a shock-tube. The steel ratio effect on the performance of the retrofits was also studied numerically. Increasing the steel ratio was found to be effective in preventing bar rupture, while this failure mode was more likely under repeated blast loading. Liu et al. [9] investigated the damage of RC columns with various levels of corrosion deterioration subjected to blast loads. The corrosion effect was modeled by considering the deterioration of rebar diameter and yield strength, the bond strength between rebar and concrete, and the rust expansion pressure effect. The results demonstrated the increased blast damage level of RC columns with different corrosion degrees. It was also found that the blast damage mode may change from combined shear and flexural damage to substantial concrete spalling damage with the increment of corrosion degree. Abbas et al. [10] investigated the capability of RC T-beam reinforced with laced stirrups in absorbing high energy as expected in blast resistance. Transverse reinforcement using lacing reinforcement and conventional vertical stirrups were compared in terms of deformation, strain, and toughness changes of the tested beams. The lacing reinforcement was efficient and participated actively in resisting the bending moments and shear forces at the same time.

A blast wave is technically defined as a quick dissipation of energy resulting in a rapid increase in pressure. This pressure increase causes a wave known as "Blast Wave" to move at a supersonic speed that decreases as the wavefront propagates. As illustrated in fig. 1, the pressure amplitude has positive and negative areas [11]. Where " $\Delta P$ " is the overpressure,

which is the change between the ambient pressure,  $P_0$  and the maximum pressure,  $P$ . Fig. 2 illustrates three main categories of explosion waves:

Free-air bursts: The explosive charge explodes in the atmosphere; the explosion waves are imposed directly onto the building without contact with the land.

Air bursts: The explosive charge is exploded in the atmosphere; the explosion waves are imposed onto the building after first contacting the land.

Surface bursts: The explosive charge explodes nearly at the land surface; the explosion waves directly contact with the land and spread hemispherical outwards, imposing themselves on the building. Where  $H_c$  is the height of the explosion charge over ground,  $W$  is the explosion charge, and  $R_G$  is the horizontal distance between the explosive charge and the building.

Related to each blast category is a typical blast loading of the building, this paper is concerned with the free air bursts.

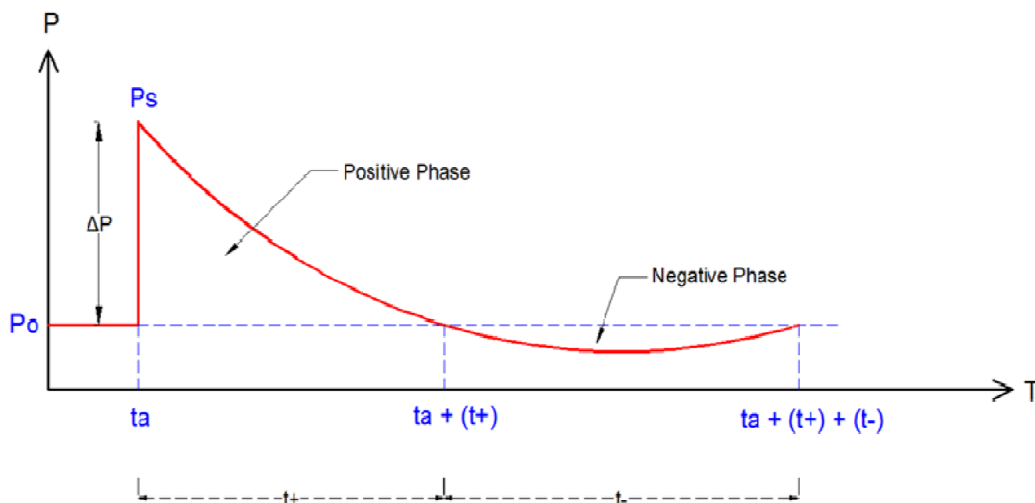


Fig. 1: Ideal blast wave behavior [11].

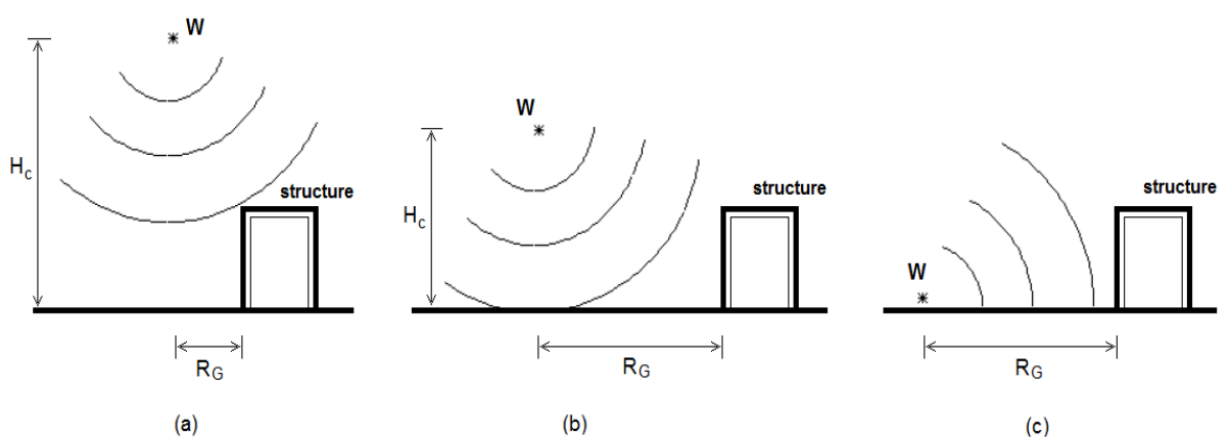


Fig. 2: Types of explosion waves: (a) Free-air bursts, (b) Air bursts, and (c) Surface bursts [12].

If two bombs have equal scaled distances, it will give the same overpressure even if it has different weight and standoff distance [3,13,14].

$$Z = \frac{D}{\sqrt[3]{W}} \tag{1}$$

Where  $Z$  is the scaled distance ( $m/Kg^{1/3}$ ),  $D$  is the distance from the bomb to the building (meter), and  $W$  is the equivalent TNT mass (Kg). UFC 3-340-02 [3] considered a scaled distance of  $0.4 m/kg^{1/3}$  as the sensitive limit for blast events. As such, blast loads with a scaled distance less than this value were considered close-in explosions. Table 1 classifies blast load events according to the scaled distance [3].

Table 1: Classification of blast events [3].

Blast load classification	Scaled distance, $Z$ ( $m/kg^{1/3}$ )	Symbol
Contact	0	C
Close-in (near)	$< 0.4$	N
Intermediate	$0.4 < Z < 1$	I
Far	$> 1.0$	F

Once the blast wave achieves the beam, as shown in fig. 3, it can produce local compressive damage. As the compressive wave spreads through the beam depth and reaches the bottom surface, it reflects as a tensile wave which produces the tensile damage and the concrete spall damage at the beam bottom surface as shown in fig. 3a. The localized shear, flexural, or flexure-shear failures of RC beams could signify several strengths and periods of explosion wave. RC beams could undergo a flexural response when the explosion period is bigger than the natural vibration period of the beam as shown in fig. 3b. In this class of failure mode, the beam may undergo a plastic hinge exposed to extreme energy explosion loading with a reduction of the concrete and reinforcement strength. Conversely, RC beams exposed to explosion waves for a short period may undergo diagonal or direct shear failures as shown in fig. 3c which are affected by the boundary conditions and detonation strength. Additionally, between the flexural and shear failures, the incident of flexural-shear failure is possible as shown in fig. 3d, when the beam is exposed to a medium range of detonation strength and period [15].

### 1.1. Research significance and objectives.

Explosion testing is limited by the test site and the used number of explosives; a large-scale explosion test is not feasible. Also, the results of laboratory experiments are limited to experiments conducted with specific parameters and under specific test conditions. Therefore, numerical analysis is adopted as a research approach instead of the actual field tests. Reviewing the literature concerning the response of blast-loaded members, it was found that the current literature depends heavily on conventional finite element simulation despite the inherent complexity of finite element modeling and analysis. Recently, the adoption of machine learning modeling for predicting the behavior of many complex structural problems has emerged as a competitor to conventional exhausting, and time-consuming numerical modeling approaches. There is still a gap in extending the use of machine learning modeling to investigate the response of RC members exposed to explosions. The present study aims to participate in bridging this gap by introducing the ANN approach as a simple and effective tool for engineers to predict the response of RC beams exposed to free-air explosions for different design parameters. To achieve the present

aim, a parametric study for RC beams subjected to explosion waves is conducted using ABAQUS to understand such behavior, and to generate an extensive dataset to train an ANN model.

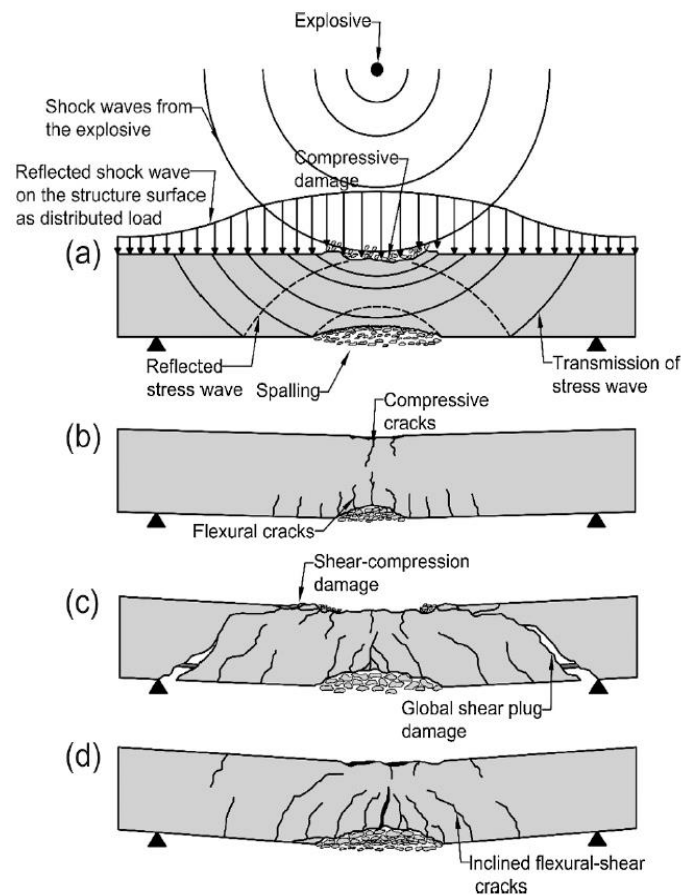


Fig. 3: failure of RC beams subjected to free-air blast loading: (a) local responses, (b) flexural failure, (c) shear failure, (d) flexural-shear failure [15].

## 1.2. Research methodology.

- 1) Simulate RC beams exposed to blast loads using ABAQUS program.
- 2) Validate the ABAQUS models using experimental data collected from the literature.
- 3) Conduct a parametric study for RC beams subjected to explosion waves using ABAQUS to understand such behavior, and to generate an extensive dataset to train an ANN model.
- 4) Develop an ANN model and prepared a graphical user interface (GUI) as a simple and practical tool for engineers to predict the behavior of RC beams exposed to explosion waves.

## 2. Nonlinear finite element analysis

Finite element modelling by ABAQUS program is used to simulate the performance of RC beams exposed to free-air explosion waves. The blast loads corresponding to the free-air

detonation of a spherical charge of TNT were generated using the Conventional Weapons Effects Program (CONWEP) definition interaction property in ABAQUS.

### 2.1. Elements modelling

The two major parts of the model were created using a solid element and a bar element to model the concrete body and the steel reinforcement respectively. The analysis step chosen was dynamic explicit. In the present study, the concrete damage plasticity (CDP) model was used to define the failure criteria [16], this model works with static and dynamic load conditions. CDP model provides a general capability for modelling concrete and other quasi-brittle materials, which is a plasticity based constitutive model utilizes a plasticity limit to assess the damage and to analyze the failure of the concrete. Damage plasticity model can simulate the cracking, crushing, and spalling of concrete. Two types of failure mechanisms are found in CDP model i.e., tensile cracking and compressive crushing, which are represented by two damage variables (for undamaged material and completely damaged material) and are responsible for the reduction in stiffness.

Steel reinforcement behaviour is described as elastic-perfectly plastic. The concrete and the reinforcement geometry were modelled as solid deformable and wire deformable element respectively. The concrete beam was meshed as structural elements of 8-nodes hexahedral linear brick element (C3D8R), while the steel reinforcement was meshed with 2-nodes linear truss element (T3D2). The constraint embedded region option was modelled as an interaction between concrete and steel. The concrete was chosen as the host region and the steel reinforcement as an embedded region. The blast loads were generated using the CONWEP definition interaction property in ABAQUS. For the boundary conditions of the beam, the two ends were pinned.

### 2.2. Material modelling

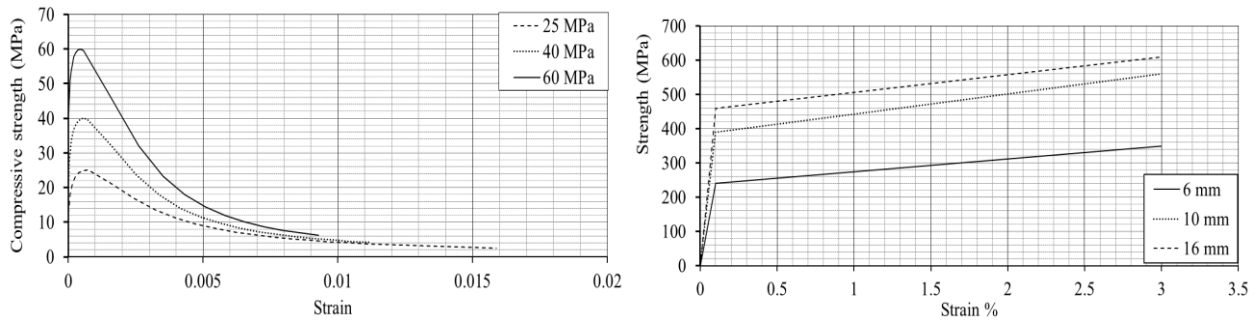
Experimental studies were used to determine the material properties of concrete and reinforcement. ABAQUS was used to simulate the material properties collected from the experimental studies. Tables 2 and 3 illustrate the concrete and reinforcement properties used for modeling. Elastic parameters like Young's modulus and Poisson's ratio of concrete are entered for the studied concrete grades, see fig. (4-a). Plastic behaviour of concrete was defined in finite element modelling using CDP model. Yield and ultimate strength of reinforcing steel are shown in fig. (4-b).

Table 2: Concrete properties used for ABAQUS models.

Compressive strength (MPa)	Elastic modulus (MPa)	Poisson ratio	Density (Kg/m3)
25	28471	0.2	2500
40	33350	0.2	2500
60	37880	0.2	2500

Table 3: Steel reinforcement properties used for ABAQUS models.

Diameter	Elastic modulus (MPa)	Poisson ratio	Density (Kg/m <sup>3</sup> )	Yield strength (MPa)	Ultimate strength (MPa)
6 mm	200000	0.3	7850	240	350
10 mm	200000	0.3	7850	390	560
16 mm	220000	0.3	7850	460	610



(a) Behavior of concrete under compression. (b) Strength-strain relationship for reinforcement.

Fig. 4: Concrete and steel behavior used for ABAQUS models.

### 2.3. Validation of finite element models

Experimental data were collected from literature [17,18] to validate the ABAQUS models. The collected experimental blast protocols used for verification are presented in Tables 4, 5. Zhang, D., et al. [17] conducted an experimental study on RC beams subjected to blast loading, beams dimensions were 100 x 100 x 1100 mm, reinforcement was 6 mm in diameter, stirrups spacing was 60 mm, concrete's compressive strength was 40.45 MPa, and yield and ultimate strengths of reinforcement steel were 395 and 501 MPa, respectively. The explosion protocol of experiments is given in Table 4.

Table 4: Blast protocol of concrete beams [17].

Model	Dimension (mm)	TNT mass (kg)	Standoff distance (m)	Scale distance (m/kg <sup>1/3</sup> )
B2-1	100x100x1100	0.36	0.4	0.57
B2-4		0.75	0.4	0.40

Table 5: Blast protocol of concrete beams [18].

Model	Dimension (mm)	TNT mass (kg)	Standoff distance (m)	Scale distance (m/kg <sup>1/3</sup> )
S12-1-2	220x300x2000	1	0.50	0.5000
S12-2		2	0.65	0.5159
S12-3		3	0.65	0.4507

Liu, S., et al. [18] investigated the blast responses of RC beams. Dimension of the beams was 220 x 300 x 2000 mm, tensile and compression reinforcement each were two HRB400 steel bars of 12 mm diameter. Stirrups were 8 mm @150 mm, and 8 mm @80 mm. Yield strength and elastic modulus were 458 MPa and 193 GPa, respectively. Concrete material

grade was C40. The beam was simply supported by 100 mm of overhang at each edge. The TNT was placed at the beam's midspan, the blast protocol is listed in Table 5.

A confident agreement between mid-span deflection of the experimental specimens and the ABAQUS models was set as the convergence criteria. Mesh size had been modified until the numerical results were almost identical and agreed with the experimental results. The optimal mesh size was 20 mm for the concrete element, while the steel reinforcement was meshed with a 5 mm mesh size. Mid-span deflection of the experimental specimens and the ABAQUS models are listed in Table 6. Results were agreed, which indicates the validity of the finite element simulation.

Table 6: Maximum deflection for experimental and ABAQUS models.

Ref.	Model	Max. deflection (mm)		Absolute Error
		Experimental	ABAQUS	
[17]	B2-1	9	9.07	0.078
	B2-4	40	37.45	0.066
[18]	S12-1-2	3.31	3.12	0.057
	S12-2	4.89	5.06	0.035
	S12-3	11.14	11.06	0.007

#### 2.4. Finite element parametric study

ABAQUS program was then employed as a nonlinear finite element analysis tool to conduct a parametric study of RC beams subjected to explosion waves. Beams' dimension was 150 x 250 x 2500 mm. The compressive and transverse reinforcement were 10 and 6 mm in diameter respectively, and the diameter of the tensile reinforcement was 10 or 16 mm. The stirrups spacing was variable between 100 and 200 mm. The concrete and reinforcement properties are given in Tables 2 and 3. The explosives were positioned over the mid-point of the RC beam as shown in fig. 5. The considered parameters in the study are as follows, and the studied parameters ranged within the values given in Table 7:

- 1) The characteristic compressive strength of concrete  $f_{cu}$ .
- 2) TNT weights.
- 3) The standoff distance (D).
- 4) Transverse reinforcement ratio  $\rho_T\%$ .
- 5) Longitudinal reinforcement ratio  $\rho_L\%$ .

According to the limitations of UFC code given in Table 1, models with TNT weights of 1.5, 8, or 5 Kg used with a standoff distance of 400 mm are considered close-in explosions. While models with a standoff distance of 1000 mm are considered intermediate explosions, and models with a standoff distance of 3000 mm are far from explosions. According to the limitations of UFC code given in Table 1, models with TNT weights of 1.5, 8, or 5 Kg used with a standoff distance of 400 mm are considered close-in explosions. While models with a standoff distance of 1000 mm are considered intermediate explosions, and models with a standoff distance of 3000 mm are intermediate explosions.



Table 7: Values used for the parametric study.

Parameter		Symbol	Value
$f_{cu}$ (MPa)		A1	25
		A2	40
		A3	60
$Z$ ( $m/kg^{1/3}$ )	TNT (Kg)	T1	1.5
		T2	8
		T3	15
	Standoff distance (mm)	D1	400
		D2	1000
		D3	3000
$\rho_L$ %		F1	0.824 %
		F2	1.467 %
$\rho_T$ %		S1	0.464 %
		S2	0.242 %

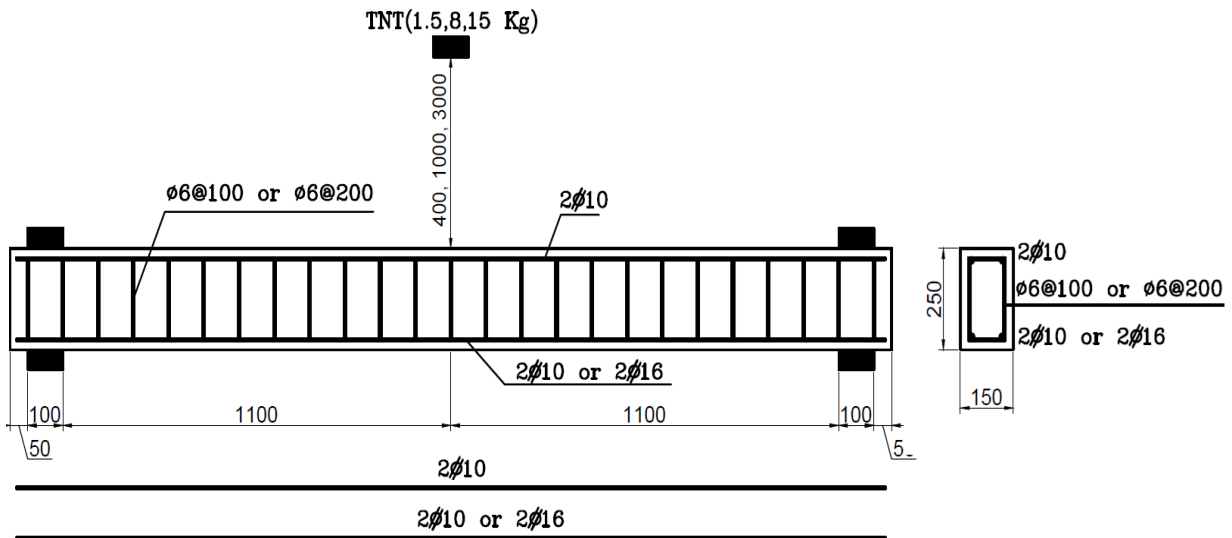


Fig. 5: Details of ABAQUS models.

### 3. Results and discussion

The conducted parametric study involved a total of 108 beam models exposed to blast loads. The models were symbolled, and the results are given in Table 8. Parameters such as mass of TNT, standoff distance, compressive strength of concrete, longitudinal reinforcement ratio, and transverse reinforcement ratio had been considered. The maximum deflection ( $Y_{max}$ ), maximum reaction forces ( $F_{max}$ ), ultimate stress ( $S_u$ ), ultimate strain ( $\epsilon_u$ ), and damage mode for beams are discussed in this section against the considered parameters.

Table 8: Maximum deflection, reaction forces, stress, strain, and damage mode of models.

Models	Y <sub>max</sub> mm	F <sub>max.</sub> KN	S <sub>u</sub> MPa	ε <sub>u</sub> *10 <sup>3</sup>	Damage mode	Models	Y <sub>max</sub> mm	F <sub>max.</sub> KN	S <sub>u</sub> MPa	ε <sub>u</sub> *10 <sup>3</sup>	Damage mode
A1= 25 MPa											
T1D1F1S	5.02	356.5	18.1	1.84	Spallin	T1D1F2S	4.55	350.1	19.0	1.77	Spallin
T1D2F1S	1.43	206.7	16.4	0.06	Cracks	T1D2F2S	1.32	202.8	15.4	0.07	Cracks
T1D3F1S	0.29	54.99	2.83	0	Intact	T1D3F2S	0.28	48.62	2.82	0	Intact
T2D1F1S	143.7	272.2	5.2	4.12	Fractur	T2D1F2S	108.0	339.8	4.09	8.66	Fractur
T2D2F1S	10.38	436.7	16.8	0.72	Spallin	T2D2F2S	9	240.5	17.7	0.4	Spallin
T2D3F1S	1.62	190.5	14.3	0.07	Cracks	T2D3F2S	1.5	182.4	12.8	0.02	Cracks
T3D1F1S	436.6	253.4	0.63	57.7	Fractur	T3D1F2S	282.3	190.1	0.56	41.9	Fractur
T3D2F1S	33.4	186.7	14.2	0.61	Spallin	T3D2F2S	29.64	263.8	18.8	1.26	Spallin
T3D3F1S	2.85	302.1	18.0	0.15	Cracks	T3D3F2S	2.64	277.6	17.4	0.13	Cracks
T1D1F1S	5.18	346.6	17.9	0.98	Spallin	T1D1F2S	4.89	334.6	20.6	1.03	Spallin
T1D2F1S	1.41	207.4	16.9	0.08	Cracks	T1D2F2S	1.35	196.4	14.7	0.08	Cracks
T1D3F1S	0.28	57.57	2.88	0	Intact	T1D3F2S	0.28	51.11	2.62	0	Intact
T2D1F1S	175.1	234.1	2.73	11.3	Fractur	T2D1F2S	133.6	299.6	2.02	14.1	Fractur
T2D2F1S	10.8	395.5	17.8	0.49	Spallin	T2D2F2S	9.64	274.1	17.1	0.32	Spallin
T2D3F1S	1.63	192.2	13.1	0.03	Cracks	T2D3F2S	1.51	184.1	12.8	0.04	Cracks
T3D1F1S	450.2	240.4	0.56	74	Fractur	T3D1F2S	357.0	162.4	0.54	51.2	Fractur
T3D2F1S	39.1	162.3	11.3	1.48	Spallin	T3D2F2S	35.99	205.9	20.0	0.61	Spallin
T3D3F1S	2.86	302.3	17.4	0.15	Cracks	T3D3F2S	2.65	282.2	18.0	0.1	Cracks
A2= 40 MPa											
T1D1F1S	3.89	471.6	31.9	0.26	Spallin	T1D1F2S	3.46	470.3	29.3	0.56	Spallin
T1D2F1S	1.33	235.0	17.7	0.1	Cracks	T1D2F2S	1.29	216.5	17.5	0.04	Cracks
T1D3F1S	0.26	53.72	3.25	0	Intact	T1D3F2S	0.24	50.17	3.05	0	Intact
T2D1F1S	130.3	324.2	3.71	5.86	Fractur	T2D1F2S	98.09	447.8	1.68	7.67	Fractur
T2D2F1S	7.77	547.9	26.8	0.41	Spallin	T2D2F2S	6.63	446.1	27.6	0.14	Spallin
T2D3F1S	1.41	168.9	16.4	0.04	Cracks	T2D3F2S	1.32	159.4	15.1	0	Cracks
T3D1F1S	438.6	316.6	0.6	53.2	Fractur	T3D1F2S	330.6	185.9	0.38	128	Fractur
T3D2F1S	23.55	451.9	25.2	1.07	Spallin	T3D2F2S	21.14	294.2	25.7	0.42	Spallin
T3D3F1S	2.41	316.3	23.4	0.02	Cracks	T3D3F2S	2.22	325.7	23.6	0.07	Cracks
T1D1F1S	4.14	466.2	30.6	0.35	Spallin	T1D1F2S	3.71	470.4	30.7	0.39	Spallin
T1D2F1S	1.33	242.8	17.5	0.05	Cracks	T1D2F2S	1.28	193.5	15.5	0.01	Cracks
T1D3F1S	0.26	52.71	3.16	0	Intact	T1D3F2S	0.25	47.8	2.93	0	Intact
T2D1F1S	150.1	312.9	2.53	7.36	Fractur	T2D1F2S	107.9	485.1	1.95	8.35	Fractur
T2D2F1S	8.22	533.3	26.5	0.14	Spallin	T2D2F2S	7.19	432.8	27.1	0.12	Spallin
T2D3F1S	1.42	165.4	16.8	0.04	Cracks	T2D3F2S	1.32	162.0	14.5	0	Cracks
T3D1F1S	433.3	276.5	0.51	79.1	Fractur	T3D1F2S	305.5	210.4	0.31	44.4	Fractur
T3D2F1S	25.21	374.3	29.5	0.2	Spallin	T3D2F2S	23.34	220.7	23.4	0.3	Spallin
T3D3F1S	2.42	320.5	24.6	0.03	Cracks	T3D3F2S	2.23	330.2	23.2	0.02	Cracks
A3= 60 MPa											
T1D1F1S	3.21	576.1	45.0	0.06	Spallin	T1D1F2S	3.06	591.7	43.0	0.06	Spallin
T1D2F1S	1.25	226.5	23.2	0	Cracks	T1D2F2S	1.14	206.2	24.6	0.01	Cracks
T1D3F1S	0.24	44.14	3.56	0	Intact	T1D3F2S	0.23	41.54	3.28	0	Intact
T2D1F1S	87.36	415.3	7.17	3.69	Fractur	T2D1F2S	89.08	471.9	1.56	18.9	Fractur
T2D2F1S	6.81	577.4	35.6	0.04	Cracks	T2D2F2S	5.87	546.7	37.3	0.03	Cracks
T2D3F1S	1.2	137.2	16.7	0	Cracks	T2D3F2S	1.12	150.9	16.5	0	Cracks
T3D1F1S	403.0	391.2	0.76	27.2	Fractur	T3D1F2S	298.1	451.9	0.78	43.2	Fractur
T3D2F1S	19.68	724.5	35.4	0.82	Spallin	T3D2F2S	16.09	563.4	45.1	0.09	Spallin
T3D3F1S	2.05	353.9	26.2	0.04	Cracks	T3D3F2S	1.9	336.6	28.2	0.04	Cracks
T1D1F1S	3.38	571.7	48.5	0.23	Spallin	T1D1F2S	3.2	595.4	39.6	0.17	Spallin
T1D2F1S	1.22	230.9	24.3	0	Cracks	T1D2F2S	1.15	212.9	22.5	0	Cracks

Models	$Y_{max}$ mm	$F_{max.}$ KN	$S_u$ MPa	$\epsilon_u$ *10 <sup>3</sup>	Damage mode	Models	$Y_{max}$ mm	$F_{max.}$ KN	$S_u$ MPa	$\epsilon_u$ *10 <sup>3</sup>	Damage mode
T1D3F1S	0.24	42.76	3.56	0	Intact	T1D3F2S	0.24	40.81	3.28	0	Intact
T2D1F1S	119.6	352.8	1.99	5.5	Fractur	T2D1F2S	95.97	509.7	3.41	3.19	Fractur
T2D2F1S	7.05	568.7	34.2	0.03	Cracks	T2D2F2S	6.11	549.2	37.3	0.04	Cracks
T2D3F1S	1.21	146.1	18.3	0	Cracks	T2D3F2S	1.13	152.9	19.9	0.01	Cracks
T3D1F1S	411.4	356.0	0.88	70.6	Fractur	T3D1F2S	265.8	294.7	0.55	38.0	Fractur
T3D2F1S	20.48	675.8	28.9	1.21	Spallin	T3D2F2S	17.59	452.3	39.8	0.05	Spallin
T3D3F1S	2.04	344.8	25.3	0.03	Cracks	T3D3F2S	1.91	341.5	26.6	0	Cracks

### 3.1. Failure modes and cracks patterns

In blast load event, energy dissipation is achieved through inelastic deformations produced by steel yielding and concrete crushing. According to ductile detailing, reinforced concrete members can resist a wide range of far, near, and close-in blast loads causing varying levels of damage. Design standards and codes (i.e., UFC) guarantee blast energy to be dissipated through inelastic deformations satisfying stated aims of performance to prevent brittle failure modes.

In the present study, different failure modes for RC beams exposed to explosion waves are obtained, see fig. 6. Beams showed mixed damage modes of both local damage and global flexural failure. For large-scaled distance of 2.62 m/kg<sup>1/3</sup> (see fig. 6 for D=3000 mm and TNT=1.5 Kg), blast waves have almost no influence on beams, they are still intact, and the deflection is 0.29 mm at maximum, as given in Table 8 for T1D3 Models. Cracks occurred at the beam centre for scaled distance range of 1.5:0.87 m/kg<sup>1/3</sup>, the maximum deflection range was 1.43:2.86 mm. With a scaled distance range of 0.5:0.35 m/kg<sup>1/3</sup>, numerous cracks appeared near the upper supports, in addition to the appearance of diagonal and flexural cracks emerging from the bottom edge, and the concrete spalling in the upper middle part of the beam. With a scaled distance range of 0.2:0.16 m/kg<sup>1/3</sup>, the concrete core of the beam centre portion fully collapses, and models undergo fracture and excessive deformations. Results show a significant effect of the scaled distance on the damage mode of RC beams. As the scaled distance decreases, large blast waves propagate, causing high blast pressure, lead to an increase in the number of cracks until collapse is reached.

### 3.2. Deflection and reaction forces

The influence of different parameters on deflection and reaction forces of RC beams subjected to explosion waves is discussed in this section. Results are elucidated in Figs. 7-12, models with scaled distances in range of 0.2:0.16 m/kg<sup>1/3</sup> are excluded from the figures because these models undergo fracture and excessive deformations. Effect of changing the transverse reinforcement ratio ( $\rho_T\%$ ) on max deflection of beams with  $f_{cu} = 25\text{MPa}$  can be explored from Fig. 7. Increasing transverse reinforcement twice leads to a reduction in deflection with percentages that vary with changing the other parameters but not more than 17.6%. The effect of longitudinal reinforcement ( $\rho_L\%$ ) on deflection of beams can be explored by comparing figs. 7(a) and (b). An 80% increase in longitudinal reinforcement leads to a deflection decrease with percentages that does not exceed 14.7%. On the other hand, by increasing the weight of TNT, deflection increases significantly. Additionally, at 1/3 of the standoff distance, the deflection is 5-10 times. Results show the significant effect

of scaled distance on deflection compared with the effect of transverse and longitudinal reinforcement ratio.

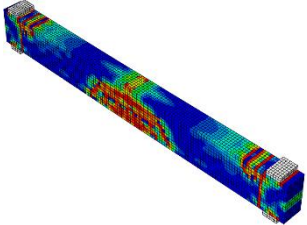
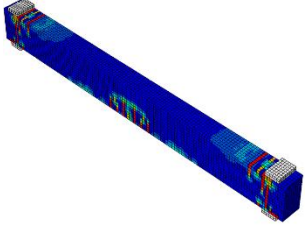

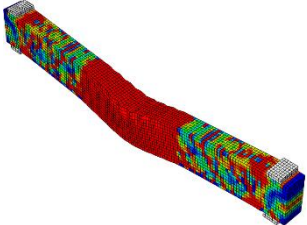
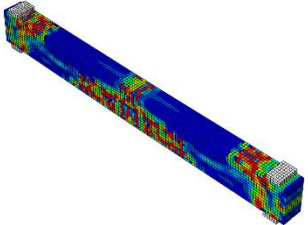
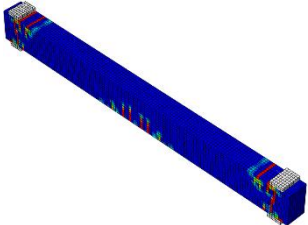
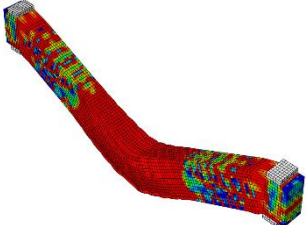
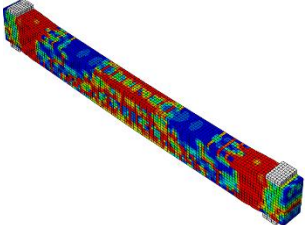
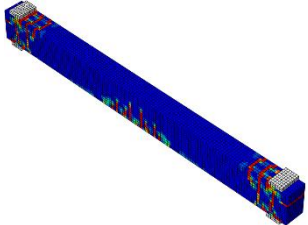
Models	D = 400 mm	D = 1000 mm	D = 3000 mm
TNT = 1.5 Kg			
TNT = 8 Kg			
TNT = 15 Kg			

Fig. 6: Damage modes of the ABAQUS models.

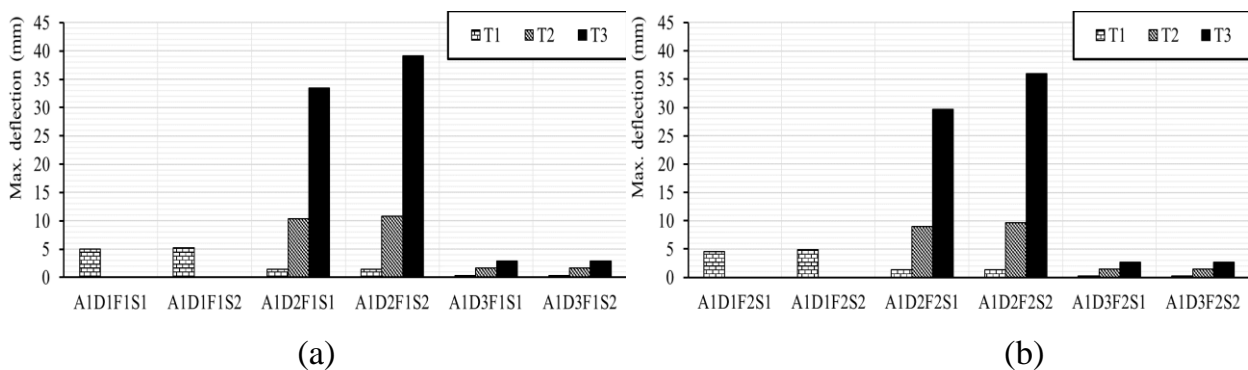


Fig. 7: Max. deflection for beams with  $f_{cu} = 25\text{MPa}$ : (a) F1 models, (b) F2 models.

The effect of transverse reinforcement ratio on resistance of beams with  $f_{cu} = 25\text{MPa}$ , represented by the max reaction forces, can be explored from Fig. 8. Max reaction forces increase with a percentage that is less than 12.3% for double transverse reinforcement ratio. By comparing figs. 8(a) and (b) it can be deduced that an 80% increase in longitudinal reinforcement causes an increase in the reaction forces with a percentage that does not exceed 13%. Increasing TNT weight greatly increases forces. With 3 times increase in standoff distance, forces decrease to 20% of its value.

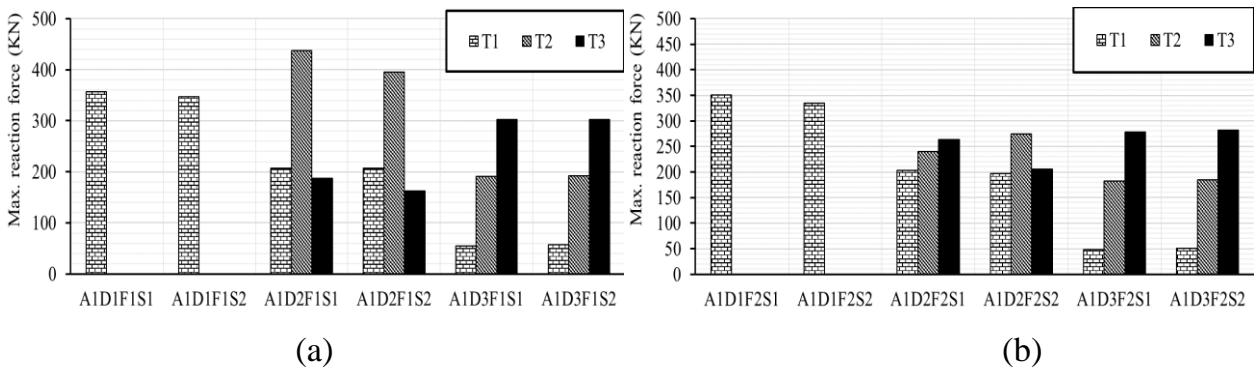


Fig. 8: Max. reaction forces for beams with  $f_{cu} = 25\text{MPa}$ : (a) F1 models, (b) F2 models.

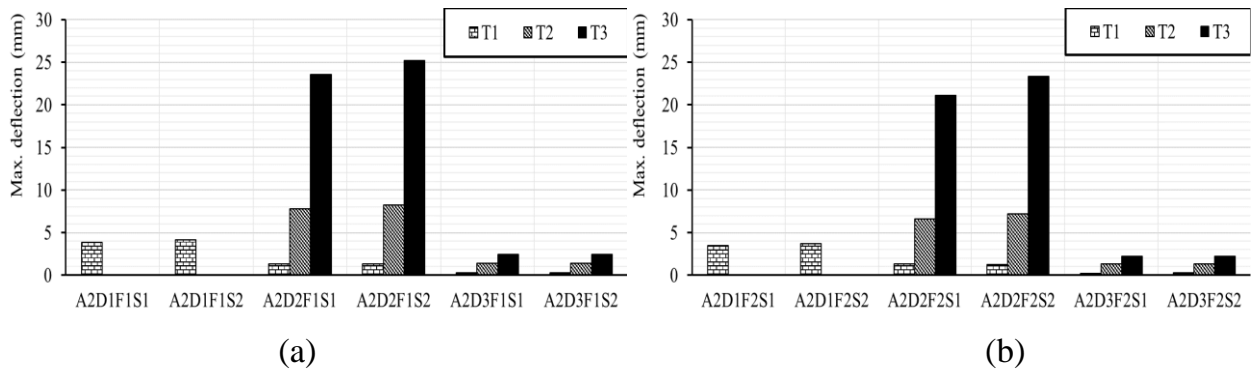


Fig. 9: Max. deflection for beams with  $f_{cu} = 40\text{MPa}$ : (a) F1 models, (b) F2 models.

Fig. 9 shows that doubling the transverse reinforcement decreases the deflection with a percentage less than 9.4% for beams with  $f_{cu} = 40\text{MPa}$ , while increasing longitudinal reinforcement decreases the deflection with a percentage less than 14%. Increasing the standoff distance decreases the deflection with percentage isn't less than 15%. Again, the scaled distance has the dominant effect on the deflection, while the effect of reinforcement ratios is weak.

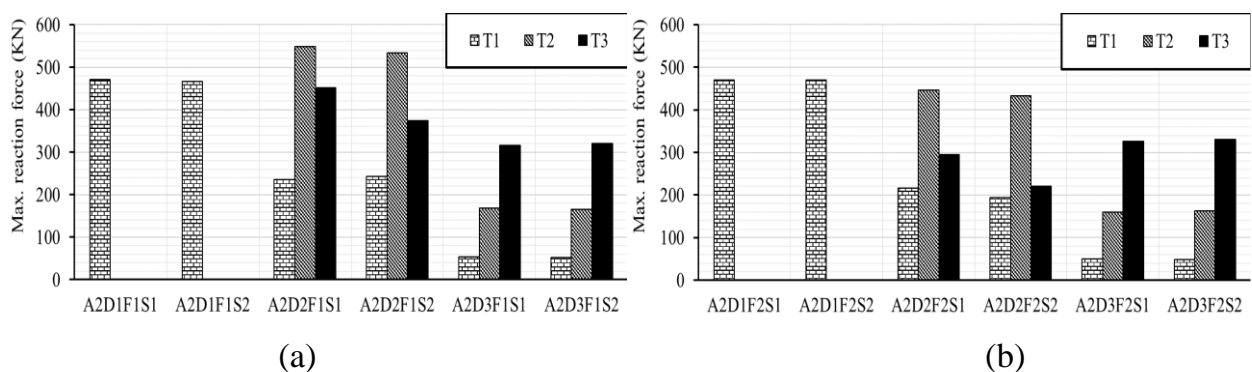


Fig. 10: Max. reaction forces for beams with  $f_{cu} = 40\text{MPa}$ : (a) F1 models, (b) F2 models.

Fig. 10 shows that, with increasing the transverse reinforcement ratio, the reaction forces increase with a percentage that does not exceed 9.5% while with increasing the longitudinal reinforcement ratio, the reaction forces increase with a percentage that does not exceed 12% for beams with  $f_{cu} = 40\text{MPa}$ .

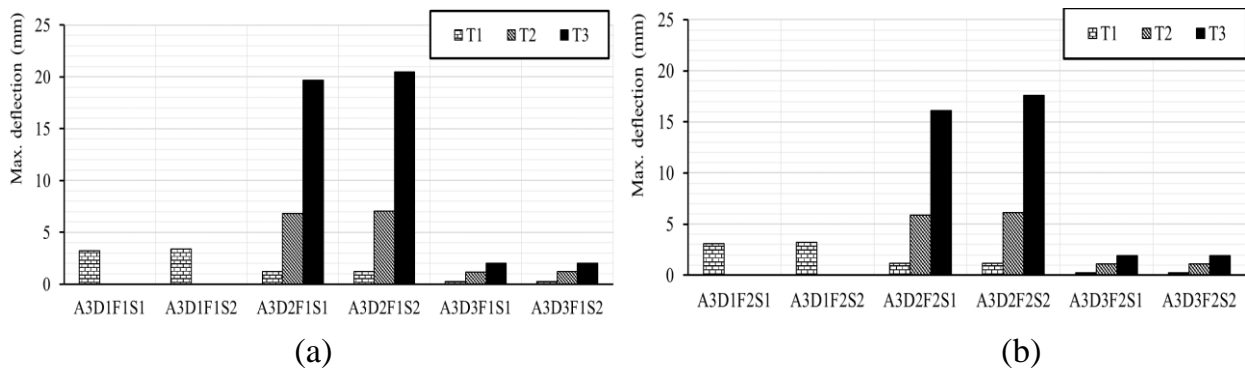


Fig. 11: Max. deflection for beams with  $f_{cu} = 60\text{MPa}$ : (a) F1 models, (b) F2 models.

Fig. 11 shows that the deflection reduction doesn't exceed 8.5% when the transverse reinforcement is doubled for beams with  $f_{cu} = 60\text{MPa}$ . Moreover, the deflection decreases with a percentage that does not exceed 13.3% when the longitudinal reinforcement ratio increases by about 80%. But with decreasing the standoff distance to one third, the deflection increases to more than five times.

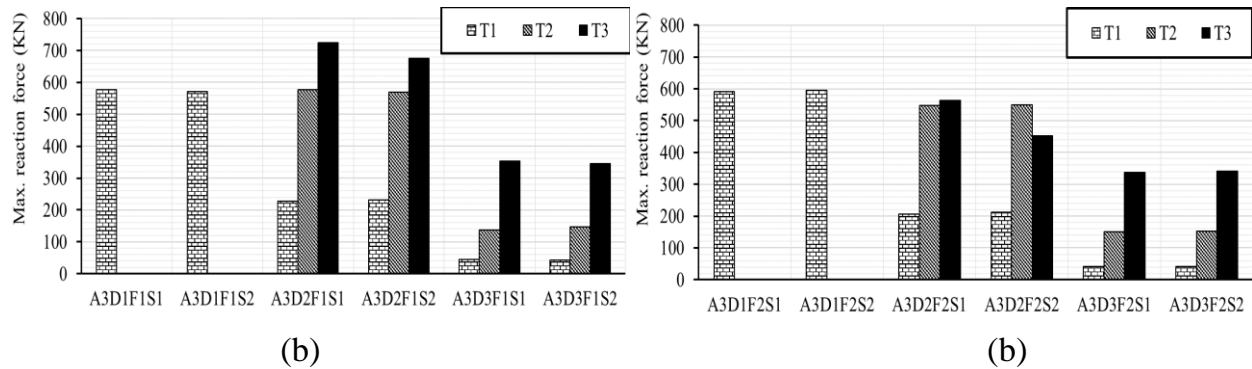


Fig. 12: Max. reaction forces for beams with  $f_{cu} = 60\text{MPa}$ : (a) F1 models, (b) F2 models.

In fig. 12, the reaction forces increase with a percentage that does not exceed 7% when transverse reinforcement ratio is doubled for beams with  $f_{cu} = 60\text{MPa}$ , while with an increase in longitudinal reinforcement ratio, the reaction forces increase with a percentage that does not exceed 3.5%.

Figs. 7-12 demonstrated the weak effect of transverse reinforcement ratio, this is due to the location of blast loads at the mid-point of the RC beam, which affects flexure behavior more than shear behavior. Likewise, changing of longitudinal reinforcement ratio is more effective with lower  $f_{cu}$  as more participation of concrete in resisting blast waves is expected for higher  $f_{cu}$ . Reviewing results from figs. 7, 9, and 11 reveals that doubling the transverse reinforcement reduced the deflection within range of 17.6%, 9.4%, and 8.5% for beams with  $f_{cu} = 25, 40,$  and  $60\text{MPa}$ , respectively, indicating that transverse reinforcement is more influencing for lower grades of concrete.

### 3.3. Ultimate stress and strain

Resistance of beams subjected to explosive waves is expressed by the ultimate stresses of concrete as given in Table 8. Results indicate that increasing transverse reinforcement ratio to double increase the beam strength in a range of 14 %. Additionally, an 80% increase in

longitudinal reinforcement leads to a strength increase with percentages that do not exceed 18 %. Moreover, increasing the concrete grade leads to a strength increase with percentages of up to 50 %. The ultimate strain of concrete at the beam centre is also given in Table 8. Results show that increasing the transverse reinforcement to double decreases the ultimate strain to about half. Additionally, an 80% increase in longitudinal reinforcement leads to a strain decrease with percentages that do not exceed 35 %. Moreover, increasing concrete strength leads to a strain decrease. On the other hand, by increasing the TNT weight or decreasing the standoff distance, the strain increases significantly.

It is quite difficult to forecast strain or load rate based on a given velocity of impact. However, if the time at which a particular stress or strain value can be measured, then the stress or strain rate can be calculated by dividing that value by the time required to achieve this value. It has been established that the modulus of elasticity is not rate-sensitive for many materials, therefore, the stress rate may be converted to strain rate by dividing the stress rate by Young's modulus [2]. In several materials, highly rapid loading rate that occurs under explosive loads leads to greater values of compression and tension strengths. Such materials are recognised as rate-sensitive materials. Concrete and reinforcing steel are rate-sensitive materials. Typical elements made of rate-sensitive materials show higher dynamic strength than static one, the strength increase links to the loading rate, the loading type, and the material characteristics. The ratio of maximum dynamic stress to maximum static stress is the dynamic increase factors (DIFs). Concrete compressive stress shows no significant strain rate sensitivity for strain rate below  $10^{-5}/s$ . When the strain rate goes beyond  $10^{-5}/s$ , the compressive strength begins to exhibit slight increases, this increase is approximately 7 to 15 %. The maximum compressive stress continues to increase reasonably until a strain rate of approximately 50/s. Beyond this strain rate, the compressive strength increases substantially as the strain rate increases [2].

In the present research, the strain rate ranges approximately  $10^{-3}/s$  to  $10/s$ . The strain rate effect for three models with different concrete grades is summarized in Table 9.

Table 9: Dynamic parameters.

Model	Compressive strength ( $f_{cu}$ ) MPa	Maximum stress ( $S_{max}$ ) MPa	Ultimate stress ( $S_u$ ) MPa	DIF
A1T1D1F1S2	25	28.78	17.94	1.15
A2T1D1F1S2	40	48.43	30.68	1.21
A3T1D1F1S2	60	66.02	48.52	1.1

Time-dependent behaviour is illustrated in Figs. 13-17. Fig. 13 illustrates the behavior developed by increasing TNT weight, the forces and the deflection significantly increase with an increase in TNT weight. Fig. 14 illustrates that with an increase in  $f_{cu}$ , the deflection slightly decreases and the resistance of the beam, represented by the reaction forces, increases. While fig. 15 shows that increasing the standoff distance causes significant decrease in forces and deflection. Minor effect of transverse reinforcement ratio is established in fig. 16; as transverse reinforcement was doubled, the deflection decreases, and the resistance increases with insignificant values. Fig. 17 illustrates the minor effect of longitudinal reinforcement on resistance and deflection. In addition, figs. 13 and 15

illustrate the increased amplitude of the deflection change with respect to time for higher TNT weight or lower standoff distance, implying higher strain rates. On the other hand, increasing the concrete compressive strength increases the amplitude and the periodic time of the deflection change, as shown in fig. 14.

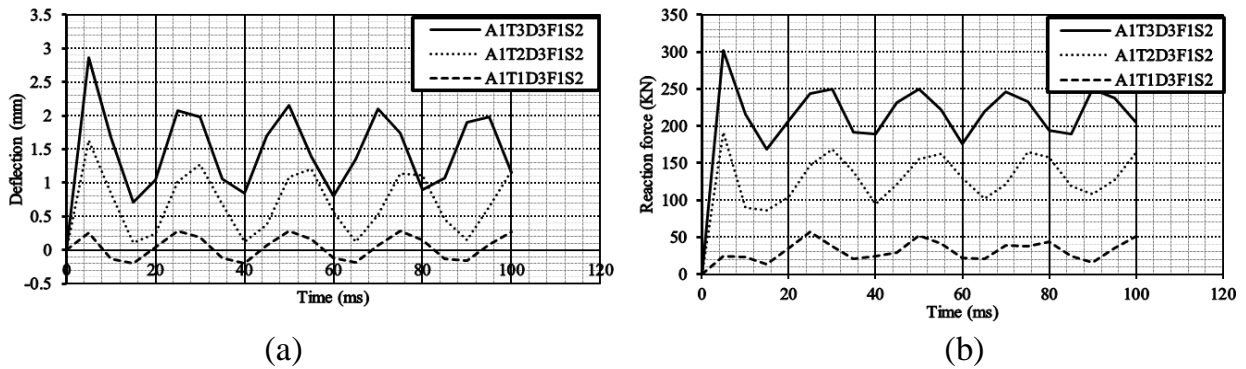


Fig. 13: (a) Deflection-time curve, (b) Reaction force-time curve for A1D3F1S2 models with a different TNT weight.

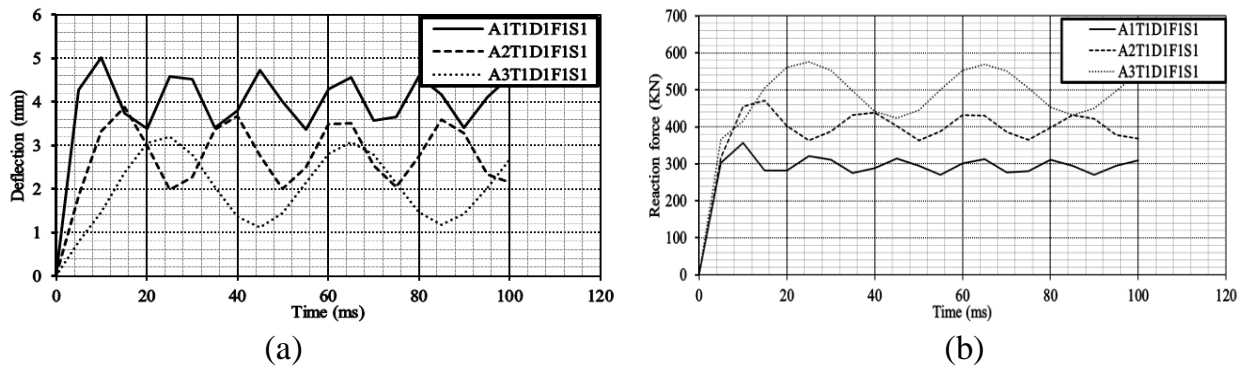


Fig. 14: (a) Deflection-time curve, (b) Reaction force-time curve for T1D1F1S1 models with a different  $f_{cu}$ .

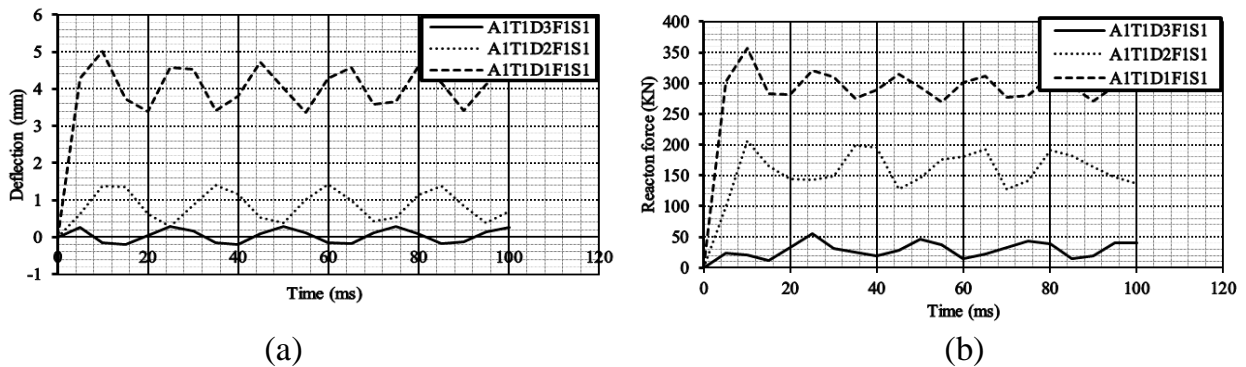


Fig. 15: (a) Deflection-time curve, (b) Reaction force-time curve for A1T1F1S1 models with a different standoff distance.



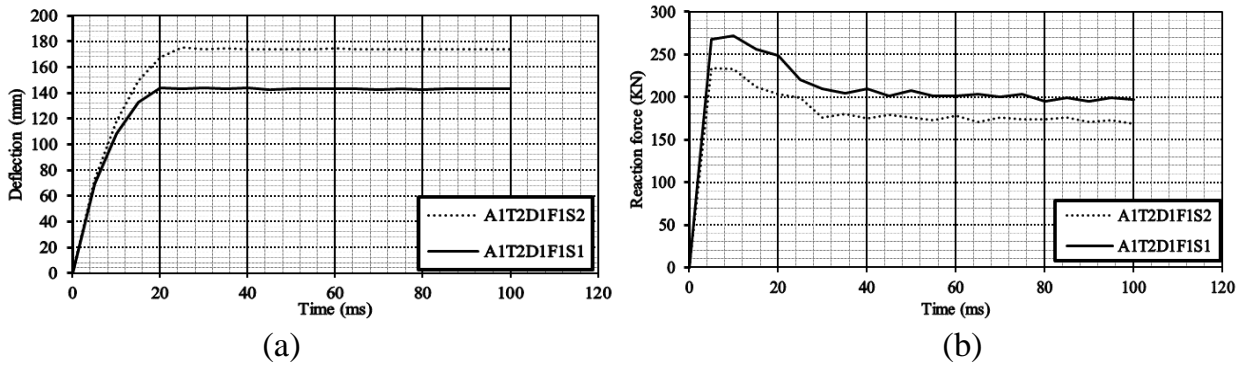


Fig. 16: (a) Deflection-time curve, (b) Reaction force-time curve for A1T2D1F1 models with a different stirrup ratio.

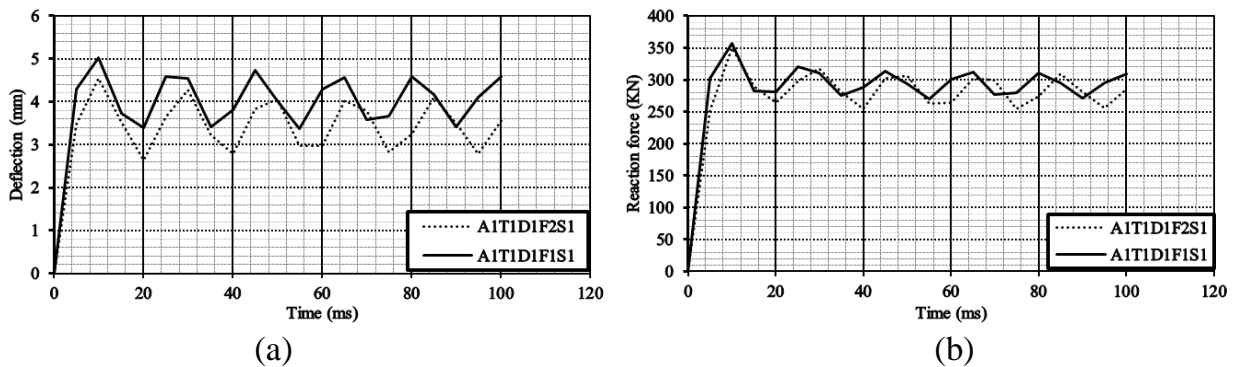


Fig. 17: (a) Deflection-time curve, (b) Reaction force-time curve for A1T1D1S1 models with different longitudinal reinforcement ratios

#### 4. Artificial neural network modelling

Artificial neural networks (ANN) are human-like mind mathematical applications, neuron is the smallest unit in an ANN model which is established in three various layers containing the input, hidden, and output layers. In this research, the ANN model utilized seven inputs, one output, and ten neurons in a hidden layer, as shown in fig. 18.

##### 4.1. Datasets preparation

314 datasets were prepared in this study using ABAQUS to train the ANN model. The model input variables are, weight of TNT, standoff distance  $D$ , concrete compressive strength  $f_{cu}$ , longitudinal reinforcement ratio  $\rho_L\%$ , transverse reinforcement ratio  $\rho_T\%$ , beam width to thickness  $b/t$ , and length to thickness  $L/t$ , as shown in Table 10. The output variable is the maximum deflection of RC beams exposed to free-air explosion waves,  $Y_{max}$ . Fig. 19 demonstrates the distribution of each variable in the prepared datasets. To construct the ANN model, the datasets were distributed arbitrarily into three groups: training, test, and validation with percentages of 70%, 15%, and 15%, respectively.

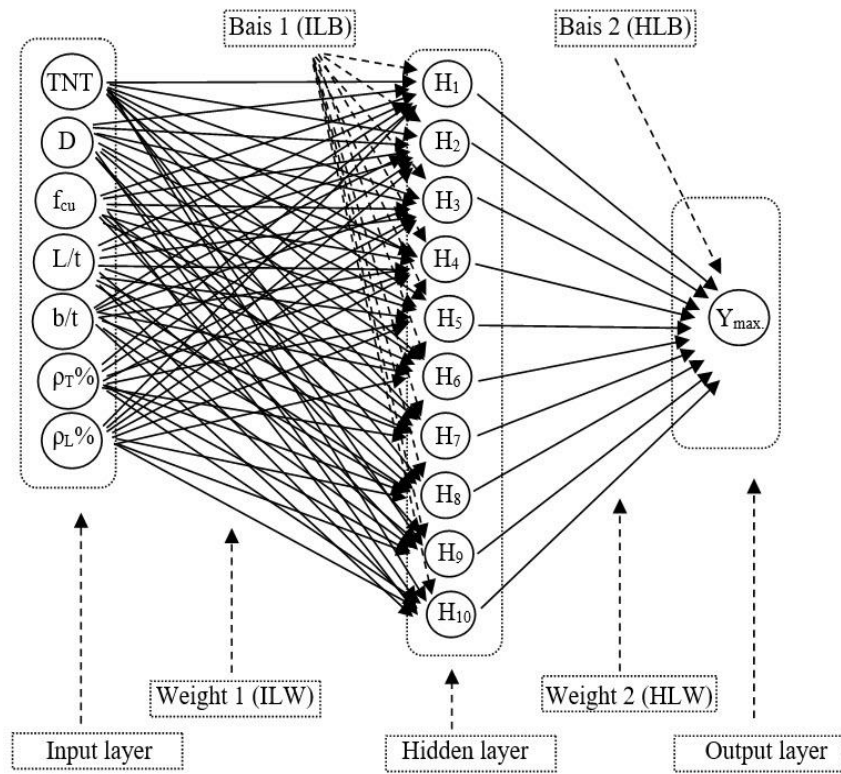


Fig. 18: Key components of the ANN model.

Table 10: Input variables of the ANN model.

Parameters	b / t	L/t	TNT (Kg)	$f_{cu}$ (MPa)	D (mm)	$\rho_T$ %	$\rho_L$ %
Values	1	10	1.5	25	400	0.464	1.467
	0.6					0.421	0.88
						0.369	0.824
	0.5	5	8	40	1000	0.298	0.734
	0.3					0.242	0.495
			0.219	0.44			
			0.192	0.412			
			15	60	3000	0.155	0.247

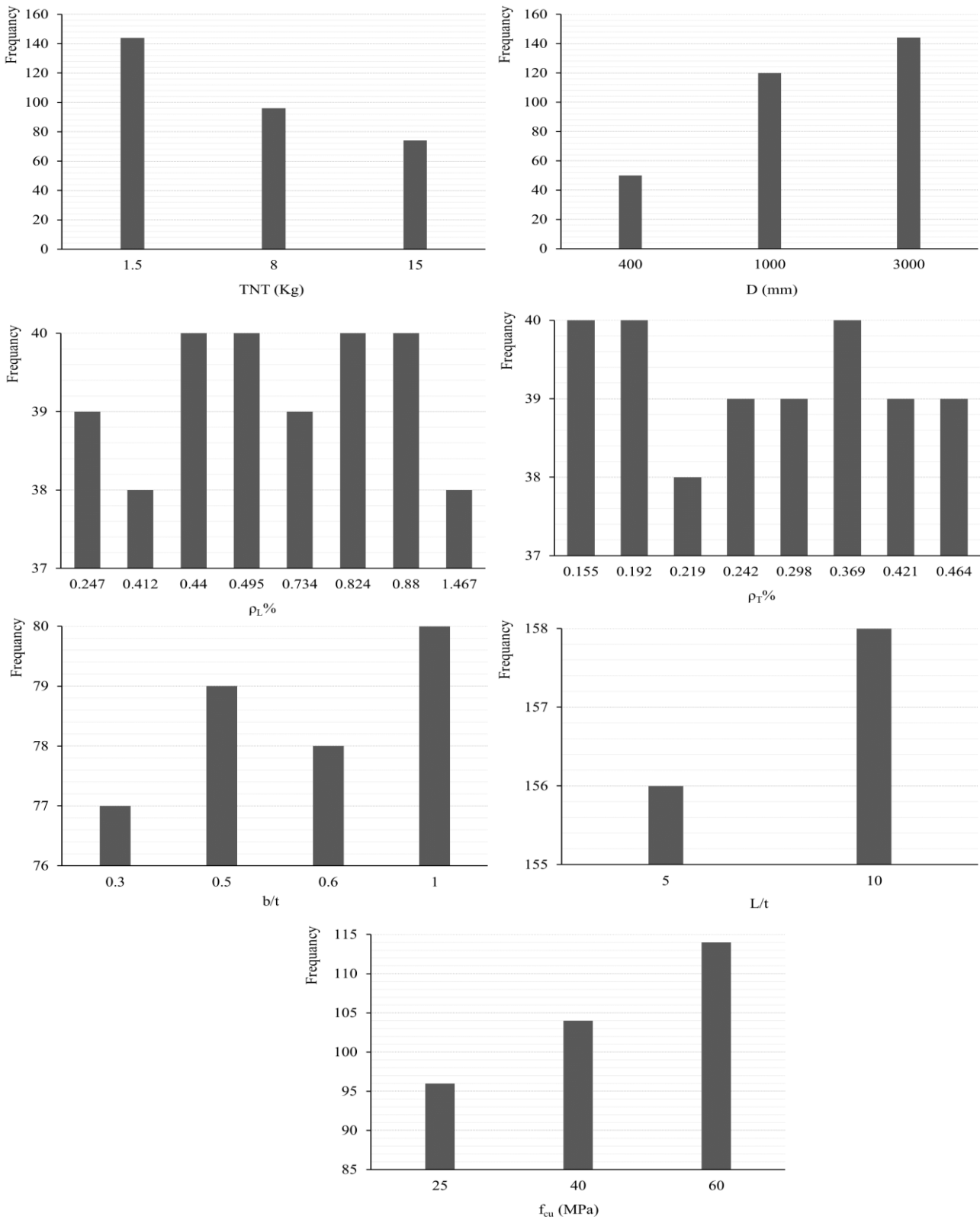


Fig. 19: Distribution of datasets information.

Fig. 20 depicts the correlation plot, which shows the relationship between input and output data, as well as the related correlation coefficients for each display. It is possible to conclude that TNT, D, L/t, and b/t are highly correlated. While  $\rho_L\%$ ,  $\rho_T\%$ , and  $f_{cu}$  are low correlated with  $Y_{max}$ .

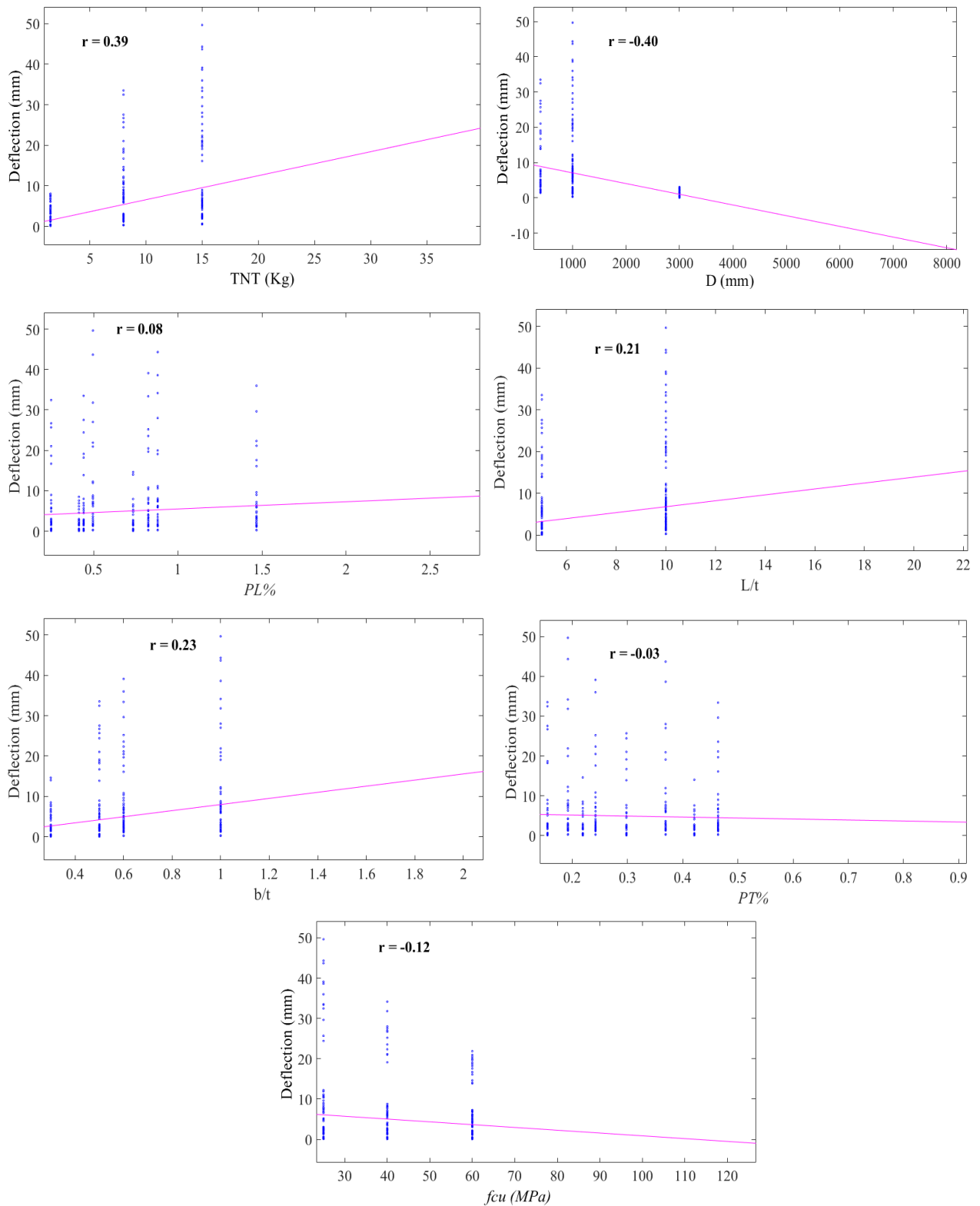


Fig. 20: Correlation plot of the datasets.

#### 4.2. Performance and Regression of the ANN Model

The standard nonlinear least squares optimization algorithm, the Levenberg-Marquardt (LM) algorithm, is extremely efficient for ANN modelling [19]. LM outperforms other algorithms in terms of generalization, convergence rate, and accuracy, and fewer iterations (epochs) are needed to get a small error. Fig. 21 illustrates the performance of the ANN

model, it displays the training, testing, and validation processes of the ANN model beginning at a big error value and declining to a smaller one. The best validation performance was found as 0.17659 with iteration 12. The least value of mean square error describes an agreeable ANN model. Fig. 22 illustrates a regression model for the ANN model that characterizes the correlation between actual and expected values.  $R = 0.99046, 0.98949, 0.98579,$  and  $0.98896$  for training, test, validation, and all data, respectively. The overall response with  $R^2$  close to one confirms that the suggested ANN model has created the optimum solutions. The suggested ANN model has agreeable performance for assessing the  $Y_{max}$  of RC beams. The ANN model may freeze after successfully training with the datasets. After that, the network is completed by calculating the output data based on new input data.

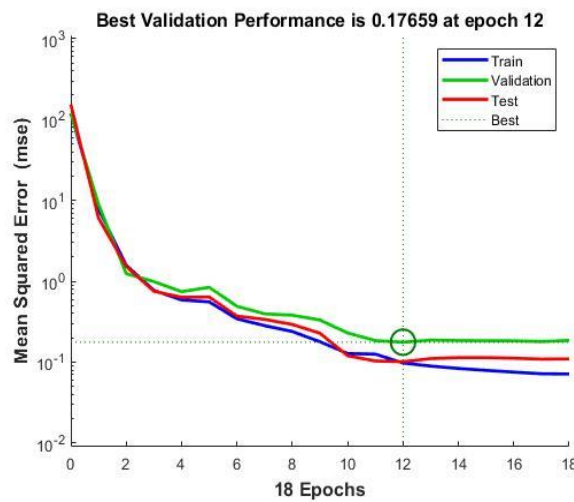


Fig. 21: The proposed ANN model's performance.

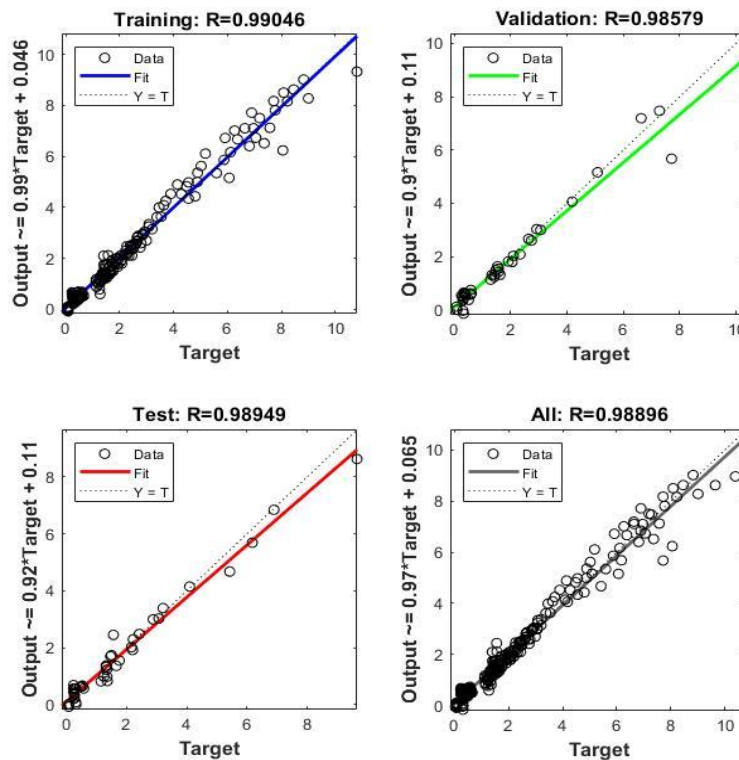


Fig. 22: The proposed ANN model's regression.

### 4.3. Verification of the ANN model

Data from literature [20-23] were collected to validate the accuracy of the ANN model in predicting the behaviour of RC beams under blast load.

Numerical simulation was presented by [20] for RC beam subjected to air blast loading. Beam dimension was 100 x 100 x 1100 mm. All specimens had a 6 mm reinforcement steel, stirrups were separated by 60 mm, compressive strength of concrete was 40.45 MPa, and reinforcement steel's yield and ultimate strengths were 395 and 501 MPa, respectively. The blast protocol is shown in Table 11.

Table 11: Blast protocol [20].

Model	Dimension (mm)	TNT mass (kg)	Standoff distance (m)	Scale distance (m/kg <sup>1/3</sup> )
B1	100x100x1100	0.3	0.4	0.598
B2		0.5	0.4	0.504
B3		0.7	0.4	0.450

A modified single-degree-of-freedom model for RC beams under explosion was presented in [21]. Beams dimension and blast protocol are shown in Table 12. The compressive and tensile reinforcement was 10 mm while 6 mm bars were used for stirrups reinforcement. The stirrups spacing was 100 mm. Concrete had a compressive strength of 41.7 MPa. The ultimate and yield strengths of reinforcement steel were 535 MPa and 420 MPa, respectively.

Table 12: Blast protocol [21].

Model	Dimension (mm)	TNT mass (kg)	Standoff distance (m)	Scale distance (m/kg <sup>1/3</sup> )
B-2	130x130x1600	1	500	0.5
B-4		3	1080	0.75

An experimental investigation was carried out to examine the dynamic responses of RC beams during close-in explosions [22]. Dimension was 200 x 200 x 2500 mm, as shown in Table 13. The compressive and tensile reinforcement were 20mm while 8 mm bars were used for stirrups reinforcement. The stirrups spacing was 150 mm. Concrete had a compressive strength of 50.16 MPa. The ultimate and yield strengths of reinforcement steel for 20 were 601.3 MPa and 466.7 MPa while for 8 mm were 582.4 MPa and 483.5 MPa respectively.

Table 13: Blast protocol [22].

Model	Dimension (mm)	TNT mass (kg)	Standoff distance (m)	Scale distance (m/kg <sup>1/3</sup> )
B1	200x200x2500	9	1.5	0.721
B2		13.4	1.5	0.632
B3		24	1.5	0.52

Experimental and analytical study were used to examine the blast performance of RC beams in [23]. Blast loading was applied to half-scale beams with dimension of 150 x 150 x 1700 mm as shown in Table 14. The compressive and tensile reinforcement were 8 mm while 6 mm bars were used for stirrups reinforcement. The stirrups spacing was 180 mm. Concrete had a compressive strength of 30 MPa.

Table 14: Blast protocol [23].

Model	Dimension (mm)	TNT mass (kg)	Standoff distance (m)	Scale distance (m/kg <sup>1/3</sup> )
B2-2	150x150x1700	0.87	0.65	0.68
B3-1		0.86	0.6	0.63
B1-3		0.8	0.5	0.54

Deflection values predicted by the ANN model and the values from literature are given in Table 15. Acceptable agreement between results demonstrated the efficiency of the proposed ANN model in predicting the behavior of RC beams under blast load.

Table 15: Maximum deflection for specimens from the literature and the ANN model prediction.

Ref.	Model	Max. deflection (mm)		Error (%)
		Experimental	ANN	
[17]	B2-3	35	35.04	0.1
	B2-4	40	43.04	7.6
	B3-1	36	36.96	2.67
[18]	S12-1-3	24.3	24.2	0.4
	S12-3	11.14	11.57	3.86
	S12-4	24.36	24.23	0.5
[20]	B1	3.5	3.78	8
	B2	7.5	6.86	9.33
	B3	10	10.36	3.6
[21]	B-2	39	38.96	0.1
	B-4	27	27.03	0.1
[22]	B1	35	35	0
	B2	39	39	0
	B3	171.83	171.83	0
[23]	B2-2	45	51.28	13.96
	B3-1	52.4	53.6	2.29
	B1-3	64.4	57.85	11.32

#### 4.4. ANN interactive graphical user interface

A graphical user interface (GUI) is prepared in MATLAB for easy usage of the proposed ANN model, as show in Fig. 23. Values of width-to-thickness of the beam  $b/t$ , transverse reinforcement ratio  $\rho_T\%$ , length-to-thickness  $L/t$ , longitudinal reinforcement ratio  $\rho_L\%$ , standoff distance  $D$ , concrete compressive strength  $f_{cu}$ , and weight of TNT are the input variables, and the maximum deflection of the beam is the output of the (GUI).

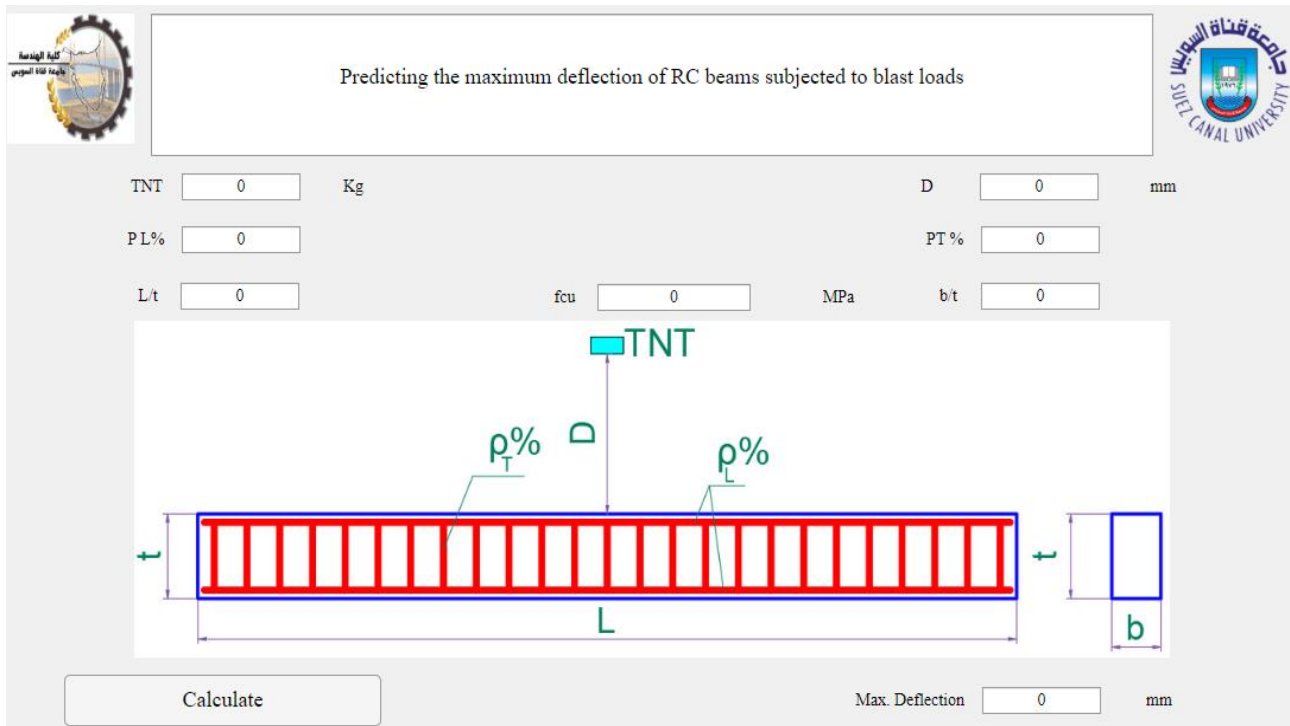


Fig. 23: ANN interactive graphical user interface.

## 5. Conclusions

This research aims at studying and modelling the response of RC beams exposed to explosion waves for various design parameters such as  $Z$ ,  $f_{cu}$ ,  $\rho_L\%$ , and  $\rho_T\%$ . The behaviour of RC beams subjected to free-air explosion waves was simulated using ABAQUS, and a parametric study was conducted. The assessed results were the deflection, reaction forces, stresses, strains, and damage modes for RC beams. An ANN model was developed using 314 numerical datasets taken from ABAQUS models. The ANN model was validated to predict the maximum deflection of RC beams. The values of width-to-thickness of the beam  $b/t$ , length-to-thickness  $L/t$ , transverse reinforcement ratio  $\rho_T\%$ , longitudinal reinforcement ratio  $\rho_L\%$ , standoff distance  $D$ , concrete compressive strength  $f_{cu}$ , and weight of TNT are the input variables, and the maximum deflection of the beam is the output of the ANN model. A graphical user interface (GUI) was prepared in MATLAB for easy usage of the proposed ANN model.

The next conclusions can be extracted from the present study:

1. The finite element ABAQUS program agrees to predict the behavior of RC beams subjected to blast loads.
2. There is no big influence on the damage mode of RC beams with different  $\rho_L\%$  and  $\rho_T\%$ , while it is severely affected by the TNT weight, standoff distance and  $f_{cu}$ .
3. Beams showed mixed damage modes of both local damage and global flexural failure.
4. For large-scaled distance of  $2.62 \text{ m/kg}^{1/3}$ , the blast waves have almost no influence on the beam and the deflection is 0.29 mm at maximum.



5. Cracks occurred at the centre area of the beams for scaled distance range of 1.5:0.87  $\text{m/kg}^{1/3}$ , and the maximum deflection range was 1.43:2.86 mm.
6. With a scaled distance range of 0.5:0.35  $\text{m/kg}^{1/3}$ , numerous cracks appeared near the upper supports in addition to diagonal and flexural cracks emerging from the bottom edge.
7. With a scaled distance range of 0.2:0.16  $\text{m/kg}^{1/3}$ , the concrete core of the beam centre portion fully collapses.
8. Results show a significant effect of the scaled distance on the damage mode of RC beams. As the scaled distance decreases, large blast waves propagate, causing high blast pressure, leading to an increase in the number of cracks until collapse is reached.
9. Increasing transverse reinforcement ratio to double leads to a reduction in deflection and increase in resistance with percentages that vary with changing the other parameters, yet, with a small value for most models.
10. Results demonstrated weak effect of the transverse reinforcement ratio, this is due to the location of the blast load at the mid-point of the RC beam, which affects flexure behavior rather than shear behavior.
11. Doubling up the transverse reinforcement reduced the deflection within range 17.6%, 9.4%, and 8.5% for beams with  $f_{cu} = 25, 40, \text{ and } 60\text{MPa}$ , respectively, indicating that transverse reinforcement is more influencing for lower grades of concrete.
12. The resistance increases by no more than 12.3% when doubling the transverse reinforcement.
13. Changing of longitudinal reinforcement ratio is more effective with lower  $f_{cu}$  as more participation of concrete in resisting blast waves is expected for higher  $f_{cu}$ .
14. The deflection decreases with a percentage that does not exceed 13.3% when the longitudinal reinforcement ratio increases by about 80%. But with 5 times increase in the TNT weight, the deflection increases to 5-6 times, and around half the standoff distance leads to 5-10 times increase in the deflection.
15. In general, the scaled distance effect on deflection and reaction forces is significant.
16. Concrete strength is significantly effective for deflection and resistance forces, with 2.5 times concrete strength,  $f_{cu}$ , the deflection decreases while the resistance increases by 52 % and 21 %, respectively, but the curves are more streamlined with increasing  $f_{cu}$ .
17. For the studied ranges of parameters, the strain rate ranged approximately  $10^{-3}/\text{s}$  to  $10/\text{s}$ .
18. The average of the dynamic increase factor is about 15% complying with ACI 370R-14.
19. For high ratios of  $L/t$  and  $b/t$  the deflection increases.
20. The suggested ANN model shows high efficiency in forecasting the deflection of RC beams under blast loads.
21. The prepared GUI is an easy yet effective tool for engineers to predict maximum deflection of RC beams exposed to blast loads.

## References

- [1] Housing and Building National Research Center, (2016), "Egyptian specification for blast resistant buildings", *SPEC 905*. Cairo.
- [2] American Concrete Institute (ACI) 370r-14, (2014), "Report for the design of concrete structures for blast effects".
- [3] Unified Facilities Criteria (UFC) 3-340-02, (2008), "Structures to resist the effects of accidental explosions", U.S. Department of Defense (DoD).  
[www.wbdg.org/ffc/dod/unified-facilities-criteria-ufc](http://www.wbdg.org/ffc/dod/unified-facilities-criteria-ufc)
- [4] Zhao, L., Hao, Y., Wang, Q., Yang, C., Yao, H., Jia, X., (2023), "Damage Zone of the Reinforced Concrete Beam under Rectangular Explosive Contact Explosions", *Buildings*, 13, 1403.  
<https://doi.org/10.3390/buildings13061403>
- [5] Gomes, G.d.J., Lúcio, V.J.d.G., Cisma,siu, C., Mingote, J.L., (2023), "Experimental Validation and Numerical Analysis of a High-Performance Blast Energy-Absorbing System for Building Structures", *Buildings*, 13, 601.  
<https://doi.org/10.3390/buildings13030601>
- [6] Robert Laszlo, Emilian Ghicioi, Florea Dinu, Calin Neagu, Dan Dubina, (2024), "Passive blast protection of buildings by ductile steel-based envelopes", *MATEC Web of Conferences*, 389, 00040.  
<https://doi.org/10.1051/mateconf/202438900040>
- [7] Chaozhi Yang, Zhengxiang Huang, Xin Jia, Wei Shang, Taian Chen, (2024), "Analytical model for predicting localized damage in RC beams under contact explosion", *International Journal of Impact Engineering*, 185, 104870.  
<https://doi.org/10.1016/j.ijimpeng.2023.104870>
- [8] Chuanjing Li, Hassan Aoude, (2023), "Behavior of UHPFRC-retrofitted RC beams with varying strengthening configurations under single and repeated blast loading", *Cement and Concrete Composites*, 142, 105180.  
<https://doi.org/10.1016/j.cemconcomp.2023.105180>
- [9] Yu Liu, Hong Hao, Yifei Hao, (2023), "Damage prediction of RC columns with various levels of corrosion deteriorations subjected to blast loading", *Journal of Building Engineering*, 80, 108019.  
<https://doi.org/10.1016/j.jobe.2023.108019>
- [10] A. Abbas, S. Arshad, G. Mohammed, Z. Ayman, I. Teghreed, A. Ali, A. Ibrahim, (2023), "Enhancement of RC T-beams toughness using laced stirrups reinforcement for blast response predictions", *Structural Concrete*, 24(3), 3839-3856.  
<https://doi.org/10.1002/suco.202200894>
- [11] Y. Temsah, A. Jahami, J. Khatib, and M. Sonebi, (2018), "Numerical analysis of a reinforced concrete beam under blast loading", *MATEC Web Conf.*, 149, p. 02063.  
[doi: 10.1051/mateconf/201814902063](https://doi.org/10.1051/mateconf/201814902063)
- [12] V. Karlos, G. Solomos, and B. Viacoz, (2013), "Calculation of blast loads for application to structural components", Luxembourg: Publications Office of the European Union, European Laboratory for Structural Assessment.  
[doi:10.2788/61866](https://doi.org/10.2788/61866)
- [13] B. Samali, G. McKenzie, C. Zhang, and E. Ancich, (2018), "Review of the basics of state of the art of blast loading", *Asian J. Civ. Eng.*, 19(7), 775–791.  
[doi: 10.1007/s42107-018-0063-y](https://doi.org/10.1007/s42107-018-0063-y)
- [14] H. Draganić, G. Gazić, and D. Varevac, (2019), "Experimental investigation of design and retrofit methods for blast load mitigation – A state-of-the-art review", *Engineering Structures*, 190, 189–209.  
[doi: 10.1016/j.engstruct.2019.03.088](https://doi.org/10.1016/j.engstruct.2019.03.088)
- [15] C. Zhang, G. Gholipour, and A. A. Mousavi, (2019), "Nonlinear dynamic behavior of simply-supported RC beams subjected to combined impact-blast loading", *Eng. Struct.*, 181, 124–142.  
[doi: 10.1016/j.engstruct.2018.12.014](https://doi.org/10.1016/j.engstruct.2018.12.014)
- [16] S. V Chaudhari and M. A. Chakrabarti, (2012), "Modeling of concrete for nonlinear analysis Using Finite Element Code ABAQUS", *International Journal of Computer Applications* (0975 – 8887), 44(7), 14–18.

- Doi: 10.5120/6274-8437
- [17] D. Zhang *et al.*, (2013), "Experimental study on scaling of RC beams under close-in blast loading", *Eng. Fail. Anal.*, 33, 497–504.  
doi: 10.1016/j.engfailanal.2013.06.020
- [18] S. Liu *et al.*, (2019), "Blast responses of concrete beams reinforced with GFRP bars: Experimental research and equivalent static analysis", *Compos. Struct.*, 226.  
doi: 10.1016/j.compstruct.2019.111271
- [19] Tran, V. L., Thai, D. K., & Kim, S. E. (2019), "Application of ANN in predicting ACC of SCFST column. Composite Structures", 228, 111332.  
<https://doi.org/10.1016/j.compstruct.2019.111332>
- [20] Y. Qu, X. Li, X. Kong, W. Zhang, and X. Wang, (2016), "Numerical simulation on dynamic behavior of reinforced concrete beam with initial cracks subjected to air blast loading", *Eng. Struct.*, 128, 96–110.  
doi: 10.1016/j.engstruct.2016.09.032
- [21] W. Wei, Y. lei Zhang, J. jun Su, Y. Liu, and F. lei Huang, (2022), "Modification of SDOF model for reinforced concrete beams under close-in explosion", *Def. Technol.*  
doi: 10.1016/j.dt.2022.01.012
- [22] B. Rao, L. Chen, Q. Fang, J. Hong, Z. xian Liu, and H. bo Xiang, (2018), "Dynamic responses of reinforced concrete beams under double-end-initiated close-in explosion", *Def. Technol.*, 14(5), 527–539.  
Doi: 10.1016/j.dt.2018.07.024
- [23] Y. Liu, J. bo Yan, and F. lei Huang, (2018), "Behavior of reinforced concrete beams and columns subjected to blast loading", *Def. Technol.*, 14(5) 550–559.  
Doi: 10.1016/j.dt.2018.07.026

## الكمرات الخرسانية المسلحة تحت تأثير الأحمال الانفجارية : المحاكاة العددية والنمذجة باستخدام تعلم الآلة

### الملخص

أصبح استخدام المتفجرات لاستهداف المباني المدنية وغيرها من المنشآت في جميع أنحاء العالم مشكلة متنامية في المجتمعات الحديثة. تركز هذه الورقة على الكمرات الخرسانية المسلحة المعرضة لأحمال انفجارية. يقدم البحث أولاً دراسة بارامترية حول سلوك الكمرات الخرسانية المسلحة المعرضة لأحمال الانفجار باستخدام محاكاة العناصر المحددة، ومن ثم تقترح نموذج الشبكة العصبية الاصطناعية (ANN) للتنبؤ بهذا السلوك بطريقة بسيطة وسهلة. تم استخدام برنامج ABAQUS لمحاكاة سلوك الكمرات الخرسانية المسلحة تحت أحمال الانفجار. تم جمع البيانات التجريبية من أبحاث سابقة واستخدامها للتحقق من صحة نماذج ABAQUS. تمت دراسة التشكل الأقصى، قوى رد الفعل، الإجهاد، الانفعال، ونوع الانهيار للكمرة. معاملات التصميم المدروسة في الدراسة البارامترية هي قوة الضغط المميزة للخرسانة ( $f_{cu}$ )، ونسبة التسليح العرضي ( $\rho_T\%$ )، ونسبة التسليح الطولي ( $\rho_L\%$ )، والمسافة المقاسة الاعتبارية للتفجير (Z). في هذا البحث تم تدريب واختبار نموذج ANN باستخدام البيانات المنتجة باستخدام برنامج ABAQUS. استخدم برنامج البرمجة (MATLAB) في استنتاج نموذج لتوقع الترخيم الأقصى للكمرة الخرسانية المسلحة المعرضة لموجات انفجارية باستخدام تقنية (ANN) معتمداً على نتائج ٣١٤ نموذج من برنامج النمذجة (ABAQUS). معاملات الإدخال لنموذج ANN هي وزن المادة المتفجرة TNT، ومسافة المواجهة (D)، وقوة الضغط المميزة للخرسانة، ونسبة التسليح العرضي، ونسبة التسليح الطولي، ونسبة عرض إلى عمق الكمرية (b/t)، ونسبة طول إلى عمق الكمرية (L/t). أظهر السلوك المتوقع باستخدام نموذج ANN مصداقية النموذج. أشارت النتائج إلى تأثير شكل ونوع الانهيار بمسافة التفجير ووزن الشحنة التفجيرية والمقاومة المميزة للخرسانة على عكس النسبة المئوية للتسليح الطولي والتسليح العرضي لا يوجد لهم تأثير ملحوظ. أظهر السلوك المتوقع باستخدام نموذج ANN مصداقية النموذج.